Manuscript version: 12 May 2020
Springer, The International Journal of Advanced Manufacturing Technology
https://doi.org/10.1007/s00170-020-05458-9

Experimental and empirical model analysis of microsurface texturing on 316 L press-fit joints fabricated by selective laser melting

H. Sohrabpoor, R. T. Mousavian, S. O'Halloran, K. Y. Benyounis, M. Baraheni, M. A. Obeidi, I. Ul Ahad, R. Raghavendra & D. Brabazon

1Advanced Processing Technology Research Centre, School of Mech. & Man. Eng, Dublin City University, Dublin, Ireland

2 I-Form, Advanced Manufacturing Research Centre, Dublin City University, Dublin, Ireland

3 SEAM Research Centre, Department of Engineering Technology, Waterford Institute of Technology, Waterford, Ireland

4 Institute of Precision Machining, Hochschule Furtwangen University, Villingen, Germany

Corresponding Author: h.sohrab@outlook.com

Abstract: In this study, selective laser melting (SLM) was investigated for the manufacturing of 316L stainless steel press-fit joints. The accuracy of selective laser melting technique in fabrication of texture profile in shape, pitch and height of microsurface texturing was examined. The resulting insertion and removal forces achieved from the produced textured pins for cold-formed high-end fixation applications were studied. The experimental results showed that the shape, pitch and height of the texture, as well as the resultant bonding strength of the joints, can be effectively set via control of the SLM processing parameters. While trapezoidal and triangular shapes of the texture lead to stronger bonding compared with oval-shaped texture profiles, the texture height was found to have a predominant effect on bond strength. To a much lower extent, larger pitch distances also resulted in higher bond strengths. A combination of abrasive and adhesive wear mechanisms was detected via examination of the inner surface of the hub into which the press fit was inserted. Along with a process map of design of the microsurface texture geometry of metal interference fit joints, this paper also presents the underlying mechanics for their bonding. The SLM process is shown to present a useful one-step method for the manufacturing of knurl metallic interference fit pins of customisable and definable texture and ensuing bond strength.

Keywords Selectivelaser melting Press-fitjoint Microsurfacetexture Response surface methodology .Box-Behnken design, Abrasive and adhesive wears

To cite this article: *H. Sohrabpoor, R. T. Mousavian, S. O'Halloran, K. Y. Benyounis, M. Baraheni, M. A. Obeidi, I. Ul Ahad, R. Raghavendra & D. Brabazon, Experimental and empirical model analysis of microsurface texturing on 316 L press-fit joints fabricated by selective laser melting, The International Journal of Advanced Manufacturing Technology volume 108, pages2687–2699 (2020).*

Manuscript version: 12 May 2020
Springer, The International Journal of Advanced Manufacturing Technology
https://doi.org/10.1007/s00170-020-05458-9

Introduction

Joining is a processing technique which is employed to assemble individual components or structures to ultimately build a larger assembly. Press fit is a joining method which provides for the easy method for the joining of materials while bonding them very securely together [1, 2]. It is commonly used, therefore, for production assembly as well as in repair applications. In recent years, press-fit joining has been used in many sectors including transportation, agricultural machineries and automotive industries. In many of these applications, it is used for increasing the capability of the joints, including the transmission of axial force from the shaft to the inner surface of a hub which is assisted through the design of the pin-hub assembly to generate defined plastic deformation and friction-related forces [3, 4]. Knurled press fits consist of two types of pins including those of straight and helical shape of texture. In straight press-fit scenarios, adhesion occurs as a result of the uniform shape of the interference pin and hub surfaces. In knurled fit joints, the pin textured surface can be designed to cut into the hub hole surface [4]. With a single helical direction of the surface profile texture, such as a single 45° knurl, the pin is guided to turn into the hub as it enters through the hole making even tighter contact with the inner surface of the hole. Therefore, radial forces resulting from helical textures effects more the interior surface of a press-fit joint compared with straight-grooved pins [4]. During the creation of a press fit, both elastic and plastic deformation occurs. The extent of deformation is directly related to the texture shape and the interfering volume of material [2]. In a press fit, the interfering volume and hence the pin's texture are important factors in bonding and adhesion of the pin to the hole, and it is crucial to know how this texture relates to the joint properties [1].

Lasers are employed across the manufacturing industry as tools capable of delivering intense cutting or welding power with high precision. CO2 lasers have been used for many applications, including drilling [5], welding [6] and texturing [7]. The dimensions of the texture and selection of an appropriate manufacturing technique that can provide these are, therefore, important considerations [7, 8]. In fact, the qualification of connection insertion force (IF) and removal force (RF) is highly sensitive to the quality of the surface texture. Obeidi et al. [9, 10] used a CO2 laser to produce surface texture on stainless steel pin insertions and measured the resulting insertion and pull-out forces. Although, this technique was successfully applied to manufacture pins with highly defined textures, the range of texture profiles could still be considered limited compared to what would be possible using metal additive manufacturing (AM) [11].

Recently, AM techniques including selective laser melting (SLM) have been used to fabricate metal parts with defined surface textures for various applications [12,13,14]. SLM can be used to fabricate samples with very complex surface textures [14, 15]. This technology represents a practical approach to many conventional fabrication methods. Based on the previous research, SLM is capable to manufacture fully dense metal parts with good mechanical properties by fusion of metallic powders [14,15,16,17]. Huang et al. [18] used this technique to fabricate 316L stainless steel (SS316L) helical microdiameter springs. They found that energy density is the most important parameter in the control of SLM product part with highest density and mechanical properties. Lin et al. [19] studied the effect of scan speed on microstructural properties of stainless steel and concluded that with an increase of scan speed, the surface roughness increased. Liu et al. [20] further found that with a scanning speed of 1000 mm/s,

stainless steel samples show higher tensile strength and ductility. Drusen et al. [21] further studied the effect of laser processing parameters on surface characterisation of 316L stainless steel fabricated by SLM using a Taguchi method for their strategy of experiments and found that higher laser energy leads to a smoother surface texture. Stainless steel is relatively low-cost and easy to process and is commonly used within both the selective laser melting and electron beam melting processes [22, 23]. Based on these characteristics, 316L was selected to fabricate the knurled joints and one of the aims of this study was to confirm the usability of this steel with metal AM for generating textures on interference fit pins to enable interference press-fit joints.

In press-fit technology, the strength of joining relies on different process parameters including the size of joint hub and pin, the surface profile dimensions and the tolerance between the joining surfaces [7, 9, 10]. Investigation of process parameters and identifying the most significant factors can be performed in different ways including with machine learning and response surface methodology [24,25,26]. The limitation of modelling data with an artificial intelligence model is the number of experiments required, which has been noted as requiring at least 300 data sets of input and output variable and is typically much larger [25]. Another solution to correlate relationship between inputs and responses is response surface methodology (RSM), which, for smaller data sets, can result in a better understanding of the impact of active factors and their interaction on the process [25]. Multiple independent variables can be examined through the RSM method which consists of a statistical and mathematical modelling of the relationship between the inputs and outputs [27]. Suman et al. [28] used the central the composite design RSM for studying the mechanical and metallurgical behaviour of weld joints and a design of experiment approach also for determining the parameters for microhole drilling [29].

Box-Behnken Design (BBD) is a great tool for investigation of the process parameters which includes three levels of inputs and, compared with other design matrices, requires a relatively smaller number of experiments [30]. The advantages offered by the RSM can be summarised as (i) determining the interaction between the independent variables, (ii) modelling the system mathematically and (iii) saving time and cost by reducing the number of trials [12]. RSM designs and, in particular, BBD perform better than other techniques when optimisation is one of the goals, as they are developed for optimisation [14].

To the best of the authors' knowledge, no research has been published on the manufacture knurled pins via SLM. In this study, the interference fit joint surfaces are accurately designed with a focus on the geometrical parameters of achievable surface profile, such as height, pitch size and shape. The output measures including the achieved profile dimensions as well as IF and RF were assessed with RSM. The main objects of this study were as follows:

1. Fabrication of press-fit textures using SLM as a potential or preferred alternative manufacturing technique compared with traditional methods.

2. To characterise the produced samples for the surface mechanical properties.

Manuscript version: 12 May 2020
Springer, The International Journal of Advanced Manufacturing Technology
https://doi.org/10.1007/s00170-020-05458-9

3. To find the most critical texturing geometrical parameters for the control of the bond strength and repeatability for insertion and removal forces using a design of experiments approach.

Experimental procedure

Material

The material used for SLM was gas-atomised spherical SS316L powder granules with a Gaussian size distribution sizes ranging from 15–50 μm (supplied by LPW Technology Ltd., UK) and had an average particle size of 27 μm (see Fig. 1), as measured using Microtrac dry dispersion laser diffraction. The chemical composition of the stainless-steel powders as supplied is listed in Table 1. The powder grains were mostly spherical in shape, while a very small number of irregular-shaped particles were revealed.

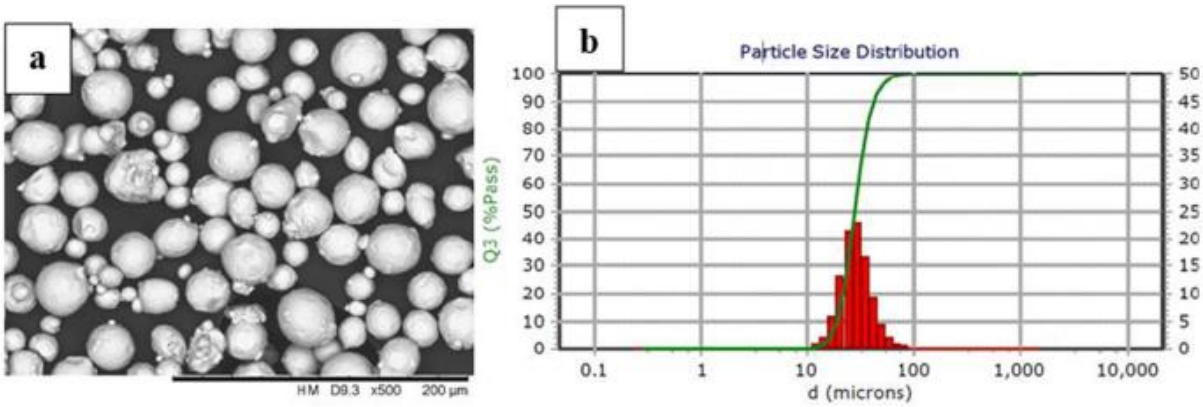

Fig:1 (**a**) SEM image. (**b**) Particle size distribution for the 316L stainless-steel powder

Table 1 Chemical composite of as supplied 316L stainless-steel powder

Chemical compositions	C	Cr	Cu	Fe	Mn	Mo	N	Ni	O	P	S	Si
Mass fraction (%)	0.023	17.7	0.01	Bal.	0.9	2.32	0.09	12.7	0.03	0.01	0.005	0.7

Equipment

The schematic of a SLM device is shown in Fig. 2a. The knurled insertion pins were manufactured using an EOS M280 metal additive manufacturing machine, as shown in Fig. 2b, using EOS default laser parameters for 316L stainless steel. The build layer thickness was set at 20 μm, and the build plate was pre-heated and maintained at a temperature of 80 °C during the building process. The starting length of the stainless-steel cylindrical samples was 30 ± 1.0 mm with a diameter of 10 ± 0.1 mm (regardless of the thickness of the texture). For each layer, the bulk material of the pin was exposed by the laser processed and then the outer counter was exposed during the SLM process; this is shown in Fig. 2c (green is the bulk material and red is the outer contour). The manufactured samples were removed from the build plate using a wire EDM (Excetek Technologies). To perform the insertion and removal test, the hubs were manufactured with a 30-mm outer diameter and 10.050 ± 0.003 mm internal diameter by means of a CNC lathe machine. The inner diameter of the hub hole was reamed to the final dimension after initial rough machining to achieve the tolerance in diameter and eliminate non-roundness.

Manuscript version: 12 May 2020
Springer, The International Journal of Advanced Manufacturing Technology
https://doi.org/10.1007/s00170-020-05458-9

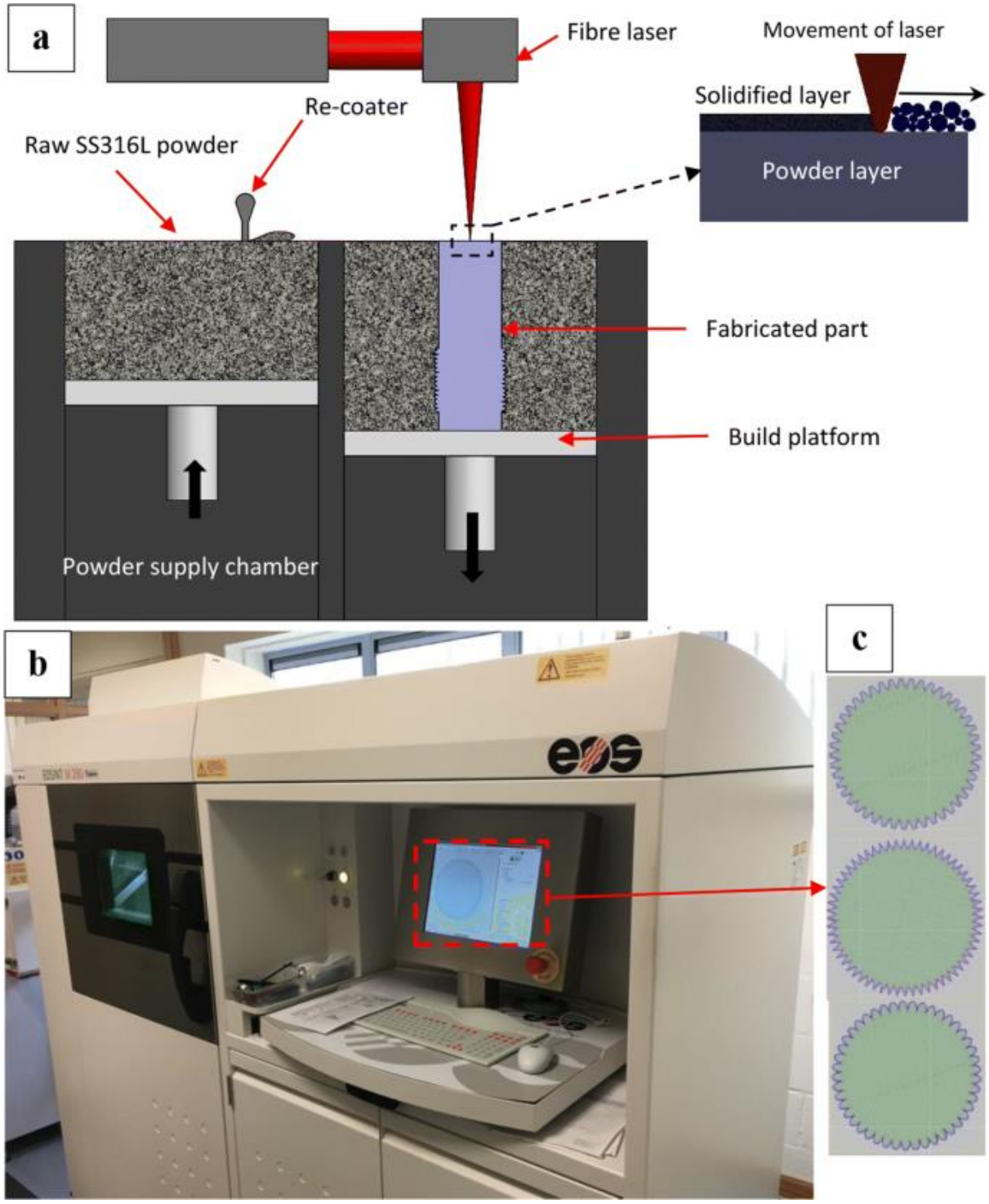

Fig.2. (a) Schematic of the SLM process. (b) EOS SLM machine. (c) Plan view of one layer of the pins with textures in the SLM control software

The dimensions of textures and surfaces were measured using a digital Vernier Caliper - Mitutoyo and Keyence 3D digital microscope (VHX2000E). The accuracy of the texture manufactured by the SLM process was within ± 5 µm in both the height and pitch dimensions. A Carl-Zeiss Scanning Electron Microscope EVO-LS15 was used to visualise the morphology of the surfaces before and after the insertion-removal tests. The experimental measurement of the texture before/after the removal tests was performed with a Keyence 3D optical

Manuscript version: 12 May 2020
Springer, The International Journal of Advanced Manufacturing Technology
https://doi.org/10.1007/s00170-020-05458-9

microscope profiler. The measured textures and outer diameters were consistent longitudinally and circumferentially. The insertion and removal forces were measured using a Zwick Z-50 tensile testing machine with the Zwick TestXpert software. The pins and hubs were vertically aligned using an upper grip and lower adjustable plate fixtures in line with the main axis of testing apparatus. The specimens were inserted, left for 30 s, and then pulled out. Both insertion and withdrawal were at a speed of 5 mm/min for all tests. Figure 3 depicts a schematic of the testing process with the Zwick Z-50. The pins and hubs were vertically aligned using an upper grip and lower adjustable plate fixtures in line with the main axis of testing apparatus. The specimens were inserted, left for 30 s, and then pulled out. For all tests, both insertion and withdrawal were at a speed of 5 mm/min.

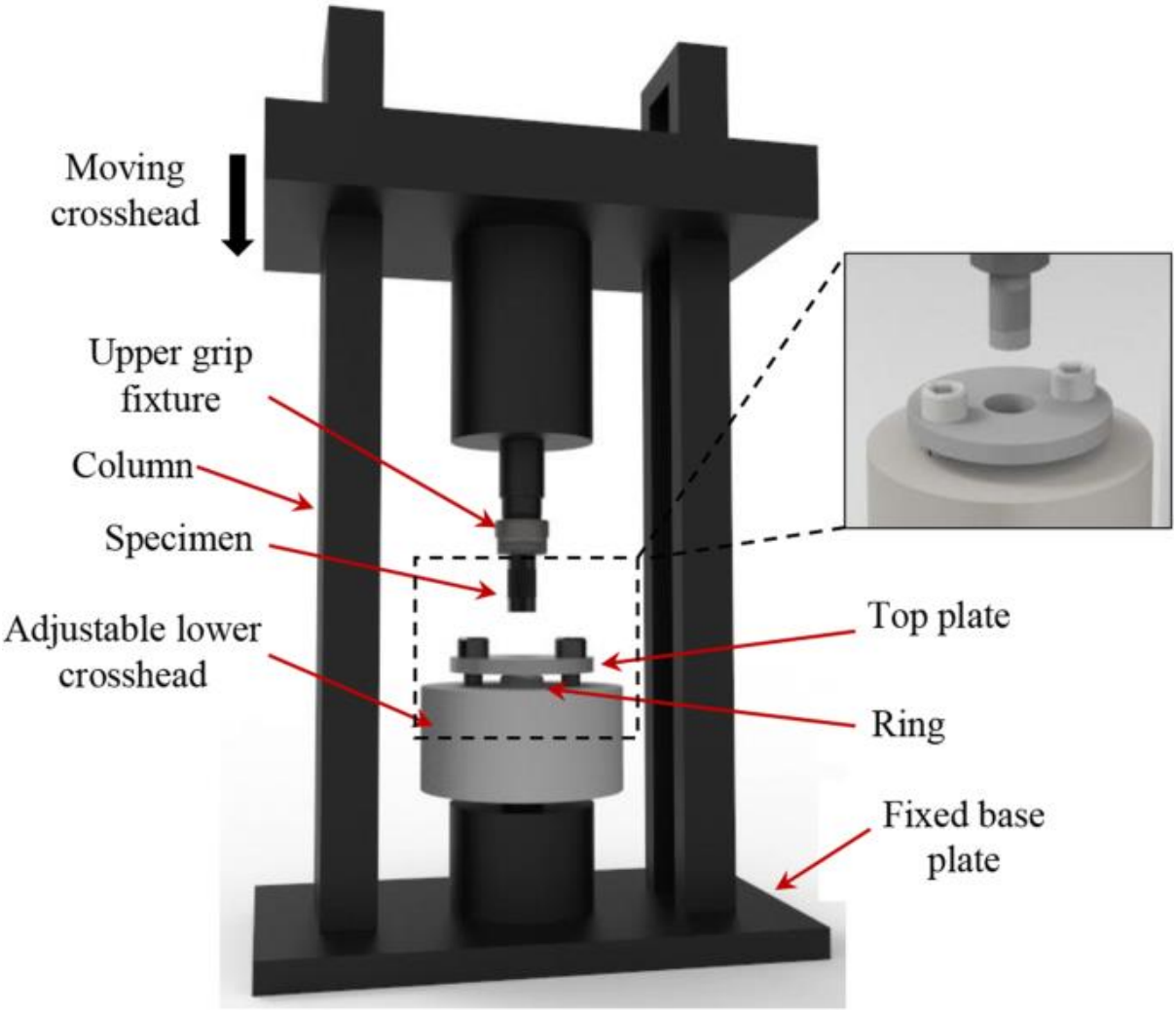

Fig. 3. Schematic of insertion and removal testing machine with fixtures and test sample in place

Design of experiment

Second-order polynomial mathematical equation has been developed by RSM to find the highest quality of output factors. Based on the equation below:

$$Y = \beta_0 + \sum_{i=1}^{k} \beta_i X_i + \sum_{i=1}^{k} \beta_{ii} X_i^2 + \sum_{i=1}^{k-1} \sum_{j=i+1}^{k} \beta_{ij} X_i X_j + \varepsilon \quad (1)$$

Manuscript version: 12 May 2020
Springer, The International Journal of Advanced Manufacturing Technology
https://doi.org/10.1007/s00170-020-05458-9

where Y represents the estimated outputs, Xi and Xj are the independent paraments and β0, βi, and βii are the intercept value, first- and second-order constant coefficients, respectively. Also, βij represents a linear constant coefficient for the connection between parameters, K is the total number of input parameters and ε is the error of the equation. Design Expert Version 9 was used to develop the mathematical models, and to verify the developed models, analysis of variance (ANOVA) and coefficient of determination (R2) were examined.

In the present study, the three predominate factors of surface texture chosen for analysis were profile shape of the texture, the pitch of the texture and the height of the texture. Table 2 shows the process geometrical parameters and the experimental design set levels. Based on a Box-Behnken design, for three independent parameters at three levels, 17 sets of geometrical parameters were investigated (see Table 3). To fit the second-order polynomial Eq. (1) with data from the experiments, a stepwise regression technique was applied.

Table 2 Set experimental process variables and their levels

Process parameters	Unit	Symbol	Code levels		
			− 1	0	1
Shape of texture	-	A	Oval	Triangular	Trapezoidal
Pitch of texture	μm	B	400	600	800
Height of texture	μm	C	300	500	700

Table 2 Set experimental process variables and their levels

Std	Shape	Pitch (μm)	Height (μm)	Insertion force (kN)	Removal force (kN)	Overall diameter (mm^2)
1	Oval	400	500	39.53	6.5	10.89
2	Trapezoidal	400	500	43.8	8.92	10.91
3	Oval	800	500	42.44	7.64	10.92
4	Trapezoidal	800	500	48.19	10.2	10.93
5	Oval	600	300	16.48	0.91	10.49
6	Trapezoidal	600	300	17.4	1.8	10.48
7	Oval	600	700	42.42	8.1	11.30
8	Trapezoidal	600	700	49.23	10.4	11.33
9	Triangular	400	300	14.8	0.73	10.46
10	Triangular	800	300	21.7	3.8	10.49
11	Triangular	400	700	45.12	9.6	11.29
12	Triangular	800	700	54.91	10.83	11.29
13	Triangular	600	500	44.22	9.31	10.89
14	Triangular	600	500	43.2	8.83	10.89
15	Triangular	600	500	41.13	6.95	10.90
16	Triangular	600	500	44	9.12	10.90
17	Triangular	600	500	40.3	7.03	10.89

Table 3 Experimental parameter sets (shape, pitch and height) and the resulting insertion and removal forces, as well as resulting volume, calculated from 3D scans and resulting diameters from Vernier measurement (with +/− 0.01 mm measurement precision)

Manuscript version: 12 May 2020
Springer, The International Journal of Advanced Manufacturing Technology
https://doi.org/10.1007/s00170-020-05458-9

Results and discussion

Development of mathematical models

Two quadratic models were generated, one relating the profile geometry to the insertion force and another relating the profile geometry to the removal force. In this study, ANOVA was utilised to examine the adequacy of the models. The results of mathematical relationships between inputs and outputs in RSM are shown in Table 4. Also, results of ANOVA for IF and RF are presented in Tables 5 and 6, respectively. In this work, for the validation of the empirical relationships, F and P values were checked. In general, the related models are significant if P values are less than 0.05 [7, 9, 10]. From the developed models, it was obtained that the order of influence of the input parameters on the output response is first the texture height, then the shape of the texture and then the pitch. Also, from Tables 5 and 6, the P values were less than 0.05, indicating that the models are statistically significant and can be used for output prediction within the range of input parameters investigated.

Table 4 Predictive equations for the force responses in terms of the actual input factors (shape: S, pitch: P and height: H)

Output	Oval	Triangular	Trapezoidal
IF	$-66.7983 + 0.0149 \times P + 0.3168 \times H - 0.0002 \times H^2$	$-63.9562 + 0.0149 \times P + 0.3168 \times H - 0.0002 \times H^2$	$-61.8483 + 0.0149 \times P + 0.3168 \times H - 0.0002 \times H^2$
RF	$-20.4313 + 0.0041 \times P + 0.0797 \times H - 0.00005 \times H^2$	$-19.0687 + 0.0041 \times P + 0.0797 \times H - 0.00005 \times H^2$	$-18.3838 + 0.0041 \times P + 0.0797 \times H - 0.00005 \times H^2$

Table 5 ANOVA results of IF

Source	Sum of squares	DOF	Mean square	*F* value	*P* value	Importance
Model	2299.5631	5	459.9126	82.4320	< 0.0001	Sign.
A-shape	49.5740	2	24.7870	4.4427	0.0385	
B-pitch	71.4013	1	71.4013	12.7975	0.0043	
C-height	1779.0613	1	1779.0613	318.8685	< 0.0001	
CA^2	396.6225	1	396.6225	71.0883	< 0.0001	
Lack of fit	38.7322	7	5.5332	0.9776	0.5425	Not sign.

Table 6 ANOVA results of RF

Source	Sum of squares	DOF	Mean square	*F* value	*P* value	Importance
Model	164.77	5	32.95	33.08	< 0.0001	Sign.
A-shape	8.87	2	4.43	4.45	0.0383	
B-pitch	5.61	1	5.61	5.63	0.0369	
C-height	125.53	1	125.53	126.02	< 0.0001	
C^2	24.30	1	24.30	24.39	0.0004	
Lack of fit	3.58	7	0.5111	0.2770	0.9332	Not sign.

The predicted R2 represents the quality of the regression model for the prediction of the outputs, with higher predicted R2 indicating a better fit, with a maximum value of 1. The determined model R2 values are presented in Table 7. In all the cases, the value of the determination coefficient is close to 1 indicating that the predicted data have good agreement with the actual experimental data. Figure 5 shows the normal probability of the studentised residuals which prove graphically how well the predicted data are fitted to the actual data for

both outputs. Although the R2 results show a high accuracy of the model, the other criteria are important for finding out the precision of the RSM model.

Responses	R^2	Adjusted R^2	Predicted R^2	Adequate precision
IF	0.974	0.9622	0.9373	25.5119
RF	0.9376	0.9093	0.88	17.0717

Table 7 Goodness of fit statistical measures for the developed IF and RF models

In Table 7, the adjusted R2 is also high which indicates the significance of the empirical relationships. It can be seen from this table that adequate precision for the IF and RF models is 25.51 and 17.07, respectively. In general, if the ratio is greater than 4, the model equations are considered to have sufficient precision [23]. Hence, the developed models can be used to navigate and predict within the design space. From Table 7, the adequacy of the models developed is then tested by using the analysis of ANOVA. By using this technique, it is found that calculated F ratios are larger than the tabulated values at a 95% confidence level; hence, the models are considered to be adequate [31]. Another criterion that is commonly used to illustrate the adequacy of a fitted regression model is the coefficient of determination (R2). For the models developed, the calculated R2 values and adjusted R2 values are above 95% and 90%, respectively. These values indicate that the regression models are adequate.

In addition, Fig. 4a and b shows the percentage of normal probability of outputs. From this graphs, the experimental data sets are approximately normally scattered. Figure 4c and d represents the predicted data against actual data for the responses. These graphs indicate the effect of the models and compare them against the random data. It can be seen from the plots that the dotted points are close to the fit line which shows the models are effective and strong for the prediction of random data.

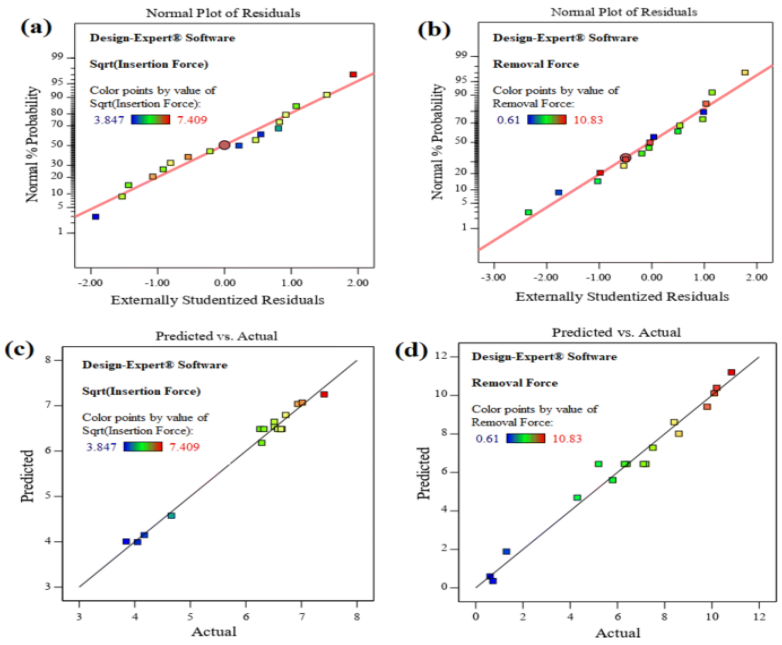

Fig: 4 Normal probability graphs of the studentised residuals for (a) IF and (b) RF, and the predicted versus actual results for (c) IF and (d) RF

Manuscript version: 12 May 2020
Springer, The International Journal of Advanced Manufacturing Technology
https://doi.org/10.1007/s00170-020-05458-9

Effects of inputs on insertion and removal force

Due to the unique specifications of the AM process, stainless-steel 316L pins were fabricated and characterised. To find the effect of shape, pitch and height, various types of pins were prepared and tested by inserting them into hubs of defined size. The IF and RF were reported, and then using RSM, the best conditions and effect of process parameters on responses for obtaining strong joints were evaluated.

Figure 5 shows the CAD designs developed using the Solidworks software version 2018 SP5, as well as the SEM morphologies of the corresponding metal AM-produced shapes. From the figures, it can be observed that due to the limitation of the manufacturing methodology of SLM process, a rough surface was formed on the external surface of texture, which would be exposed to the hub surface. It can be seen that the triangular shape has a relatively sharp edge compared with the oval shape and that the sharpness defined in the CAD schematic of the triangular shape (Fig. 5c and d) could not be achieved by the SLM process; this was due to the laser spot size and its heat-affected zone. However, both the oval (Fig. 5a and b) and trapezoidal (Fig. 5e and f) build closer to the shape of the CAD design. This highlights the requirement of knowledge of the SLM manufacturing technology during the design phase of the geometrical profiles.

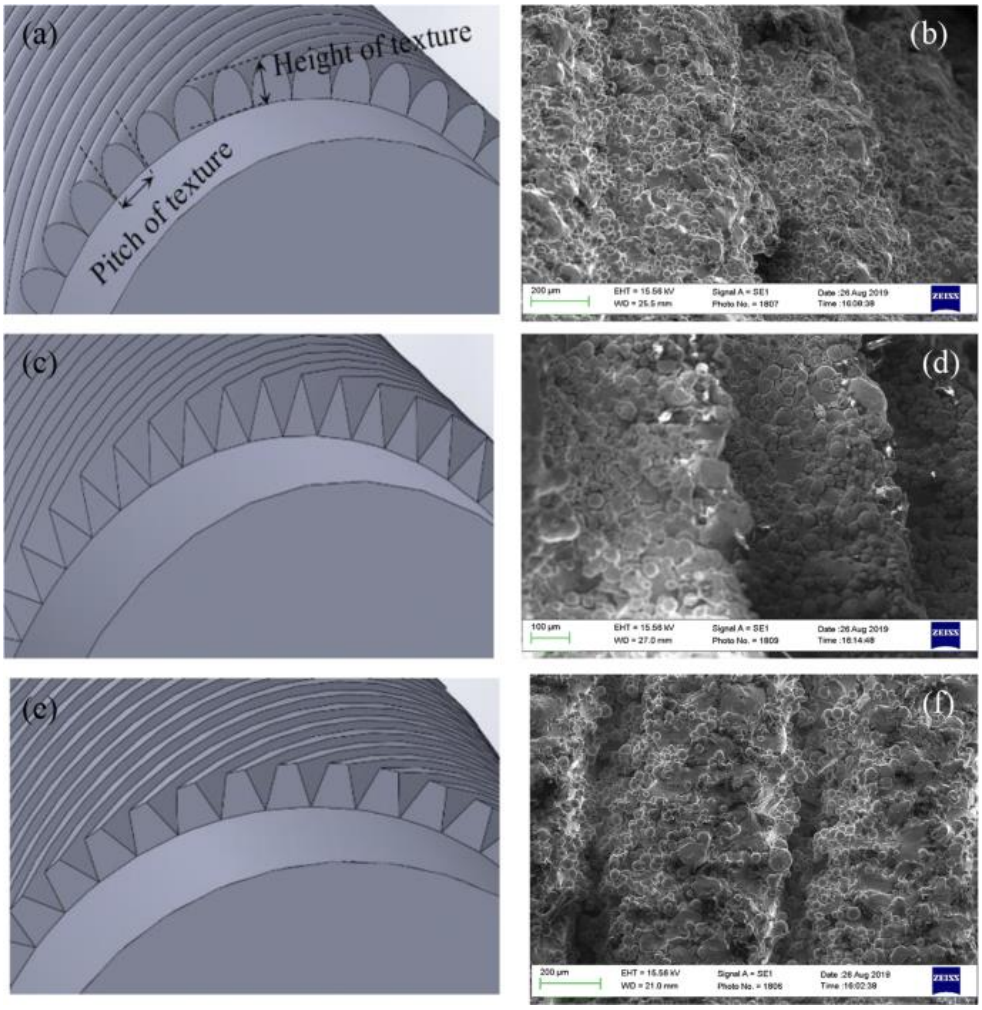

Fig 5. Schematics of the CAD designs with (**a**) oval, (**c**) triangular and (**e**) trapezoidal shapes; and respective corresponding SEM images (**b**, **d** and **f**) as-produced, before insertion tests

Manuscript version: 12 May 2020
Springer, The International Journal of Advanced Manufacturing Technology
https://doi.org/10.1007/s00170-020-05458-9

Figure 6 shows contour plots of the effects of pitch, height and shape on the IF and RF. Some important points can be drawn from this figure. First of all, as expected by increasing the height of texture, IF and RF were dramatically increased. It is important to note that before the final design of the presented texture geometries, different heights were evaluated in a set of screening experiments, and it was found that a height in the range of 300–700 μm was suitable for this application. It can also be observed that when the maximum possible height is used, there is less local response effect from the other input parameters on IF and RF. Secondly, from Fig. 6, it is seen that that the highest values of IF and RF were obtained when the shape of texture was trapezoidal. The oval shape led to the lowest levels of joint strength.

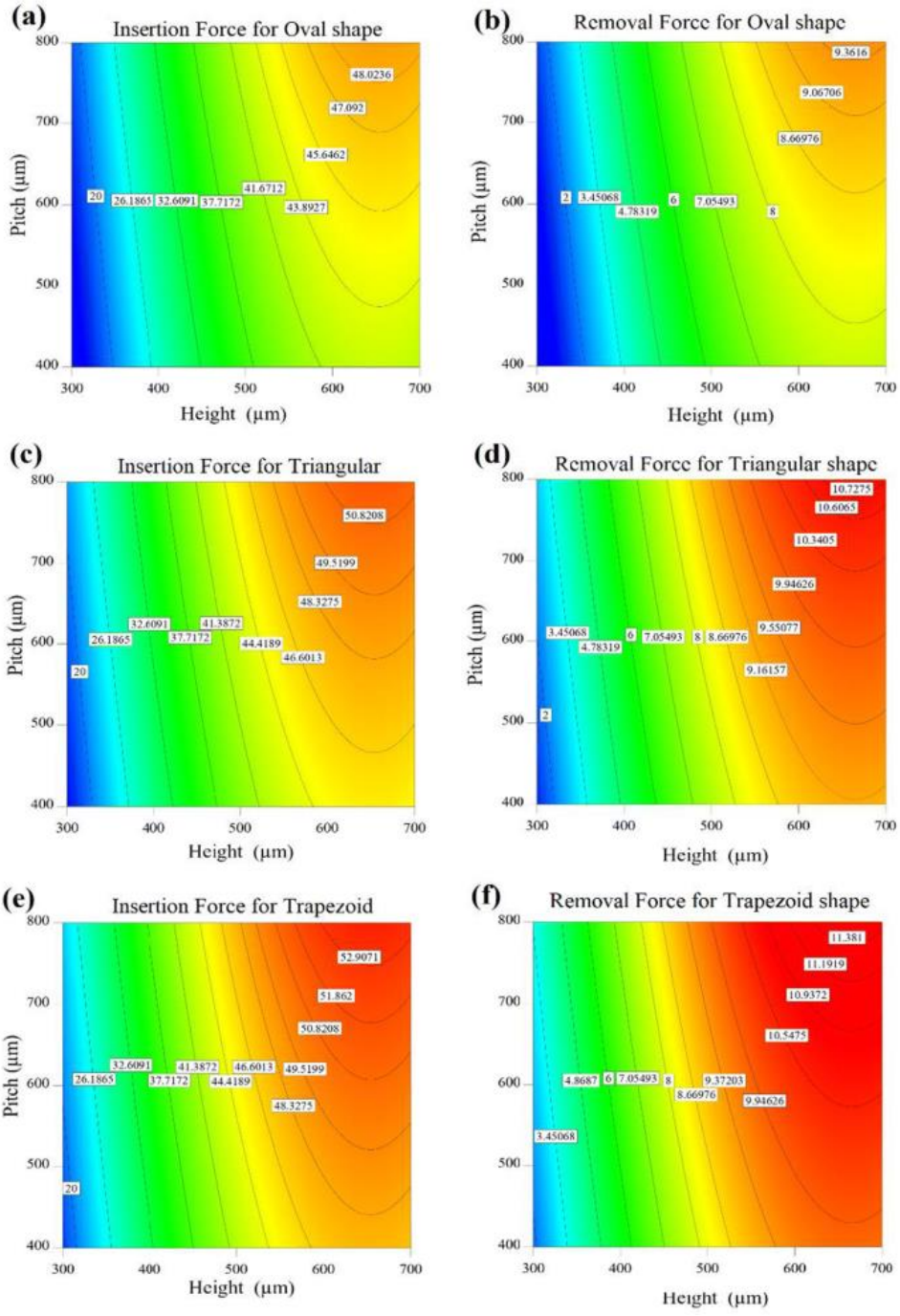

Fig 6. Colour map contour plots of IF and RF against the pitch and height, presented respectively for (a and b) oval, (c and d) triangular, and (e and f) trapezoidal shapes

Manuscript version: 12 May 2020
Springer, The International Journal of Advanced Manufacturing Technology
https://doi.org/10.1007/s00170-020-05458-9

Figure 7 shows the surface response morphology of some samples after insertion and removal, it can be expected that the triangular shape could cause more abrasive wear (see also Fig. 8), while the trapezoidal shape generated more adhesion with the inner side of hub surface technology. As can be seen from Fig. 8, there is a combination of abrasive and adhesive wear evidenced on the pin and hub surfaces after the debonding of the additively manufactured press-fit joints. From Fig. 8a, b and c, abrasive bonding was created by the sharp tooth of the triangular-shaped profile which leads to significant surface damage. This shape of texture (samples 2, 4, 6 and 8) resulted in an adhesive-type joint via interfacial and perhaps some degree of interatomic bonding (Fig. 8d, e and f). During insertion, the tooth profiles on the pin surface did not break but rather plastically deformed [32]. The most important advantage of adhesive joining compared with other bonding methodologies is that a more uniform stress distribution may be achieved via the two surfaces, with the resulting potential for better definition of the bond strength [32]. Due to the increased adhesive bonding found with the triangular shape, high insertion and removal forces were determined

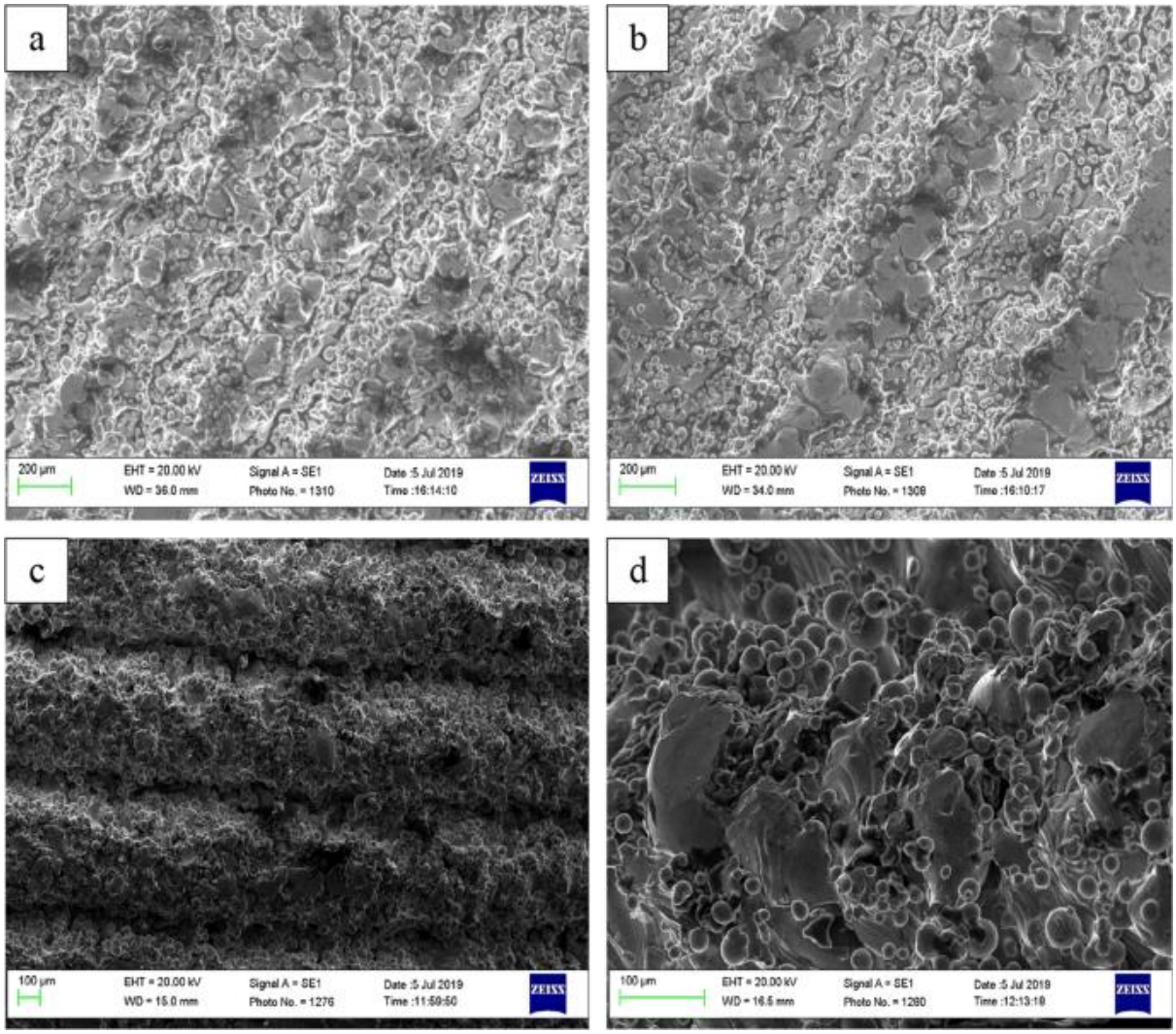

Fig 7. SEM micrograph images of the samples' surface morphologies, after insertion and removal, of (a) sample 9 (triangular shape, 400 µm pitch and 300 µm height), (b) sample 10 (triangular shape, 400 µm pitch and 300 µm height), (c) low-magnification of sample 6 (trapezoidal shape, 600 µm and 300 µm), and (d) high-magnification of sample 12 (triangular shape, 600 µm pitch and 500 µm height)

Manuscript version: 12 May 2020
Springer, The International Journal of Advanced Manufacturing Technology
https://doi.org/10.1007/s00170-020-05458-9

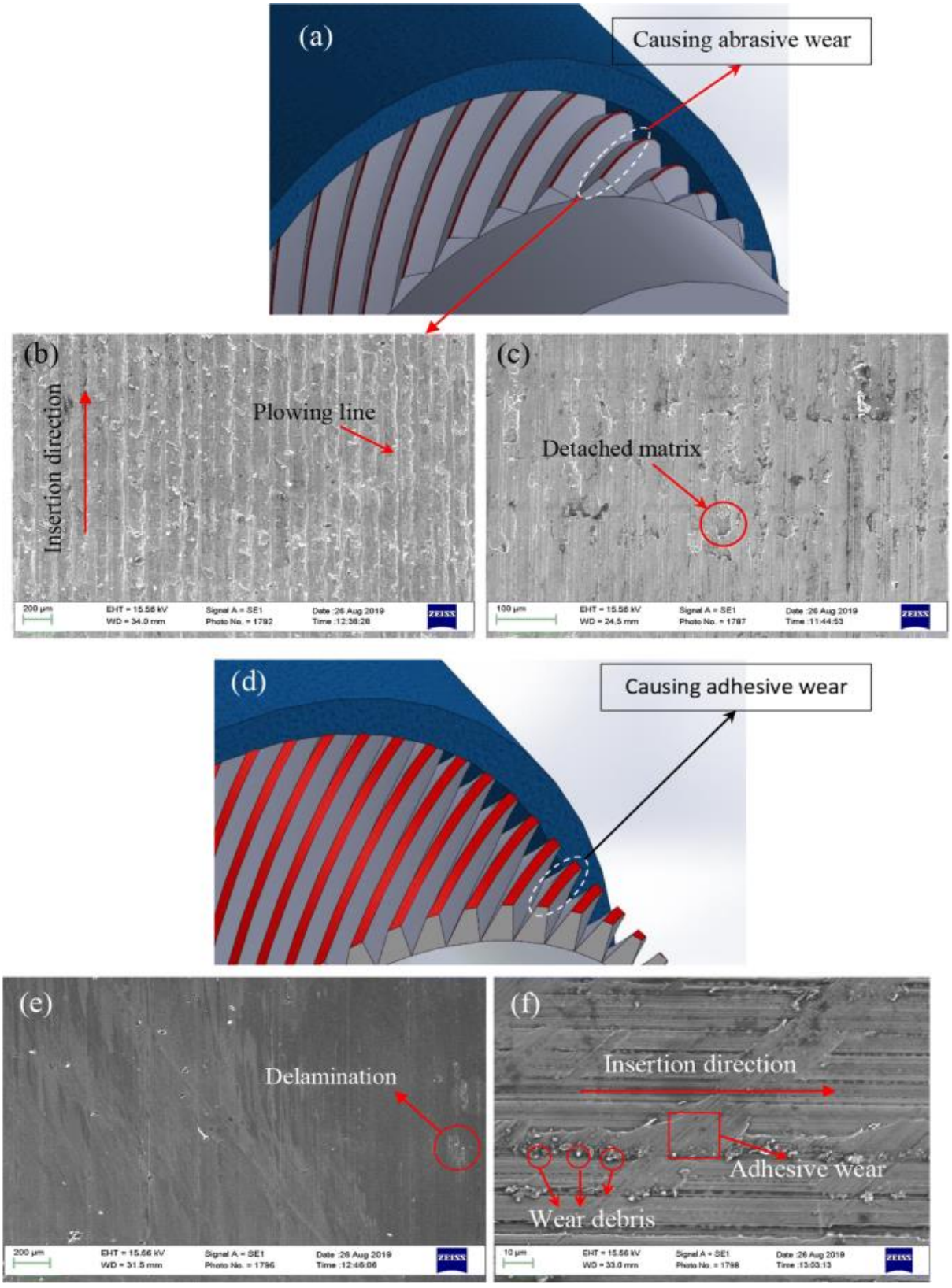

Fig 8. Schematic of (a) triangular and (d) trapezoidal textures showing in red the top surface of the texture, and (b and c) low and high magnifications of hub surface after triangular textured pin removal and (e and f) low and high magnifications of the hub after trapezoidal textured pin removal

Manuscript version: 12 May 2020
Springer, The International Journal of Advanced Manufacturing Technology
https://doi.org/10.1007/s00170-020-05458-9

Due to the relatively high as-produced surface roughness from the metal AM process (see Fig. 5b), traces of abrasive wear were detected, shown in Fig. 8. Finally, it was found that a higher pitch size leads to the maximum values of IF and RF. In Fig. 7 a and c, no considerable surface abrasion (plastic deformation) was detected for the samples 9 (triangular—pitch, 400 μm and height, 300 μm) and 6 (trapezoidal—pitch, 600 μm and height, 300 μm). It was revealed that with the triangular texture (for example sample 10), IF and RF were at maximum values, and the related sample presented in Fig. 7b showed considerable abrasion (plastic deformation) of the surface after insertion and removal. It is interesting from the higher-magnification SEM morphology of sample 6 (Fig. 7d) that the un-melted powders at the surface were smoothened due to the severe abrasion between the pin and hub surfaces during insertion and removal. It can be observed that by altering the texture parameters, strong bonds can be formed in press-fit applications. Also, AM technology can be highly recommended for such applications after a suitable surface-finish process. This study opens a new window for development of metal AM for interference fit joining applications. Future research will focus on the effect of surface-finish process after SLM to study the performance of such pins for press-fit application.

Conclusion

In summary, a new approach for the manufacturing of metallic knurled press-fit pins was developed in this study using the SLM process. The selective laser-melted specimens with different types of texture specifications were evaluated by insertion and removal tests. An RSM model was used to investigate the impact of input parameters on the bonding strength of press-fit joints. The SLM process was shown to be a one-step method for the manufacturing of customised knurl metallic pins with a complex texture shape which could eliminate the need for the precision machining of the press-fit joints. The microtexture parameters can also be selected to achieve a particular set pre-defined and more accurate level of fastening bond strength. From the experimental and simulation results, the following conclusions can be drawn:

1. It was found that the texture height was the most significant factor for resulting bond strength. The weakest bond strengths were obtained for the lowest profile heights of 300 μm and highest bond strengths were obtained for the highest profile height of 700 μm.
2. The shape of the textures affects the resulting joint bonding strength. The trapezoidal and triangular shapes of the texture lead to stronger bonding compared with oval texture profiles. The trapezoidal profile produced the highest strength bonds due to the larger interaction area between the pin surface and the internal surface of the hub
3. The pitch size also positively scaled with the bond strength but to a much lower extent than the texture height. Also, larger values of pitch resulted in higher IF and RF values.
4. The RSM is an excellent technique for the prediction of the IF and RF from the produced texture specifications. The developed process models can be reliably used to predict the resulting insertion and removal bond strengths.
5. ANOVA analysis indicated that all inputs and their interaction terms including the shape, pitch size and the height of the texture have significant effects on IF and RF outputs.

References

1.Norton RL (2011) Machine Design, Fourth edn. Pearson Education, New Jessey

2. Wanga X, Loua Z, Wang X, Xu C (2017) A new analytical method for press-fit curve prediction of interference fitting parts. J Mater Process Technol 250:16–24

3. Mengel R, Haberle J, Schlimmer M (2007) Mechanical properties of hub/shaft joints adhesively bonded and cured under hydrostatic pressure. Int J Adhes Adhes 27:568–573

4. Roche P, Wohletz S, Brenneis M, Pabst C, Resch F (2014) Joining by forming—a review on joint mechanisms, applications and future trends. J Mater Process Technol 214:1972–1994

Chatterjee S, Mahapatra SS, Mondal A, Abshishek A (2018) An experimental study on drilling of titanium alloy using CO2 laser. Sådhanå 43:131

6. Chatterjee S, Sahoo SK, Swain B, Mahapatra SS, Roy T (2020) Quality characterization of dissimilar laser welded joints of Ti6Al4V with AISI 304 by using copper deposition technique. Int J Adv Manuf Technol 106:4577–4591

7. Obeidi MA, McCarthy E, Brabazon D (2018) Laser surface processing with controlled nitrogen-argon concentration levels for regulated surface lifetime. Opt Lasers Eng 102:154–160

8. Obeidi MA, McCarthy E, Brabazon D (2016) Methodology of laser processing for precise control of surface micro-topology. Surf Coat Technol 307:702–712

9. Townsenda A, Seninb N, Blunta L, Leach RK, Taylor JS (2016) Surface texture metrology for metal additive manufacturing: a review. Precis Eng 46:34–47

10. Obeidi MA, Mccarthy E, Kailasc L, Brabazona D Laser surface texturing of stainless steel 316L cylindrical pins for interference fit applications. J Mater Process Tech 252(2018):58–68

11. Bartolomeua F, Buciumeanub M, Pintoc E, Alvesc N, Carvalhoa O, Silva AFS, Miranda G (2017) 316L stainless steel mechanical and tribological behavior—a comparison between selective laser melting, hot pressing and conventional casting. Addi Manuf 16:81–89

12. Loua S, Jiang X, Sunb W, Zeng W, Pagani L, Scott PJ (2019) Characterisation methods for powder bed fusion processed surface topography. Precis Eng 57:1–15

13. Sidambe AT, Tian Y, Prangnell PB, Foxa P (January 2019) Effect of processing parameters on the densification, microstructure and crystallographic texture during the laser powder bed fusion of pure tungsten. Int J Refract Met Hard Mater 78:254–263

14. Choo H, Sham KL, Bohling J, Ngo A, HuiXio X, Ren Y, Depond PJ, Matthews MJ, Garlead E (2019) Effect of laser power on defect, texture, and microstructure of a laser powder bed fusion processed 316L stainless steel. Mater Des 164:107534

15. Krakhmalev P, Fredriksson G, Svensson K, Yadroitsev I, Yadroitsava I, Thuvander M, Peng R (2018) Microstructure, solidification texture, and thermal stability of 316L stainless steel manufactured by laser powder bed fusion. Metals 8(8):643

16. Metelkova J, Kinds Y, Kempen K, Formanoir CD, Witvrouw A, Hooreweder BV On the influence of laser defocusing in Selective Laser Melting of 316L. Addit Manuf 23(2018):161–169

17. Bottini L, Boschetto A (2019) Interference fit of material extrusion parts. Addi Manuf 25:335–346

18. Huang M, Zhang Z, Chen P (2019) Effect of selective laser melting process parameters on microstructure and mechanical properties of 316L stainless steel helical micro-diameter spring. Int J Adv Manuf Technol 104:2117–2131

19. Lin K, Gu D, Xi L, Yuan L, Niu S, Lv P (2019) Qing Ge, Selective laser melting processing of 316L stainless steel: effect of microstructural differences along building direction on corrosion behavior. Int J Adv Manuf Technol 104:2669–2679

20. Liu J, Songa Y, Chenc C, Wang X, Li H, Zhou C, Wang J, Guo K, Suna J (2020) Effect of scanning speed on the microstructure and mechanical behaviour of 316L stainless steel fabricated by selective laser melting. Mater Des 186:108355

21. Dursun G, Ibekwe S, Li G, Mensah P, Joshi G, Jerro D (2020) Influence of laser processing parameters on the surface characteristics of 316L stainless steel manufactured by selective laser melting. Mater Today: Proc

22. Yakout M, Elbestawi MA, Veldhuis SC (2019) Density and mechanical properties in selective laser melting of Invar 36 and stainless steel 316L. J Mater Process Tech 266:397–420

23. Lawrence J (2018) Advances in laser materials processing technology, research and applications. Woodhead Publishing, Elsevier

24. Sohrabpoor H, Negi S, Shaiesteh H, Ahad IU, Brabazon D (2018) Optimizing selective laser sintering process by grey relational analysis and soft computing techniques. Optik - Int J Light Electron Opt 174:185–194

25. Chatterjee S, Mahapatra SS, Bharadwaj V, Upadhyay BN, Bindra KS (2019) Prediction of quality characteristics of laser drilled holes using artificial intelligence techniques. Eng Comput

26. Chatterjee S, Mahapatra SS, Bharadwaj V, Choubey A, Upadhyay BN, Bindra KS (2019) Drilling of micro-holes on titanium alloy using pulsed Nd:YAG laser: parametric appraisal and prediction of performance characteristics. Proc IMechE Part B: J Eng Manuf 233(8):1872–1889

27. Zhong T, He K, Li H, Yang L (2019) Mechanical properties of lightweight 316L stainless steel lattice structures fabricated by selective laser melting. Mater Des 181:108076

28. Chatterjee S, Mahapatra SS, Bharadwaj V, Upadhyay BN, Bindrab KS, Thomas J (2019) Parametric appraisal of mechanical and metallurgical behavior of butt welded joints using pulsed Nd:YAG laser on thin sheets of AISI 316. Opt Laser Technol 117:186–199

29. Chatterjee S, Mahapatra SS, Bharadwaj V, Choubey A, Upadhyay BN, Bindra KS (2018) Quality evaluation of micro drilled hole using pulsed Nd:YAG laser: a case study on AISI 316. Lasers Manuf Mater Process 5:248–269

30. Lee J, Park S, Shin K, Jung H (2018) Smearing defects: a root cause of register measurement error in roll-to-roll additive manufacturing system. Int J Adv Manuf Technol 98:3155–3165

31. Benyounis KY, Olabi AG, Hashmi MSJ (2008) Multi-response optimization of CO2 laser-welding process of austenitic stainless steel. Opt Laser Technol 40:76–87

Manuscript version: 12 May 2020
Springer, The International Journal of Advanced Manufacturing Technology
https://doi.org/10.1007/s00170-020-05458-9

32. Kolař V, Tich M, Müller M, Valašek P, Rudawska A (2019) Research on influence of cyclic degradation process on changes of structural adhesive bonds mechanical properties. Agron Res 17(S1):1062–1070